Ocean Dynamics (2004) 54: 66–76
DOI 10.1007/s10236-003-0083-2

**Hans van Haren**

# Incoherent internal tidal currents in the deep ocean

Received: 28 May 2003 / Accepted: 24 November 2003


**Abstract** 'Eleven months' current meter observations from the deep Bay of Biscay were examined for the residual (incoherent internal tidal; icIT) signal, left after harmonic analysis using eight tidal constituents (large-scale barotropic or coherent baroclinic signal) within the semidiurnal band. This residual signal comprised ~30% of the total tidal kinetic energy and, due to its flat spectral appearance, it was responsible for typically 5–7 days intermittency. Although icIT was part of the red noise internal wave band continuum, it was not attributable to instrumental noise. It consisted of quasi-harmonics at non-tidal harmonic frequencies having amplitudes larger than $N_2$, the third largest semidiurnal tidal constituent. It is suggested that the kinetic energy at these non-tidal frequencies reflects interaction between semidiurnal tidal motions and the slowly varying background conditions.

**Keywords** Residual signal · Quasi-harmonics · Tidal–background interaction

## 1 Introduction

Semidiurnal tidal motions dominate currents in large parts of the ocean, for instance near shelf edges. Tidal currents generated directly by the surface pressure gradient (barotropic tidal currents; BT) are distinguished from internal tidal currents (IT; baroclinic tidal currents), which are generated via tide–topography interaction and which are supported by density stratification in the ocean interior. Both types of motions have the same frequency, but differ strongly in characteristics like spatial scales and propagation speeds. As a result, one can expect different effects of background conditions on the different tidal motions and, specifically studied here, on their spectral shapes. Prior to studying such effects on IT, a proper separation is required of the barotropic and baroclinic currents. Due to their different scales, these currents are easily separable in theory, but less unambiguously in practice, which emphasizes the need to understand the above effects.

In theory, barotropic tidal waves are characterized by extremely narrow-band spectral shapes, being purely deterministic with well-known frequency, amplitude and phase, and wavelengths of O (1000 km) spanning major topographic structures. Their stability in frequency can be used to check clocks of instruments. However, barotropic tidal *currents* may vary over relatively short horizontal scales of O (10–100 km) and vertical scales of O (10–100 m) accommodating changes in topography (LeBlond and Mysak 1978), friction at boundaries (Maas and van Haren 1987) and horizontal density gradients or fronts (van Haren and Maas 1987). These scales are also typical for IT as these are dependent on the interaction between barotropic currents and (3-D; e.g. Munk 1997) topography, as well as on stratification.

In the deep ocean, away from internal tidal wave sources, IT exhibit strong intermittency and unstable phase (Ekman 1931; Wunsch 1975), attributed to varying background conditions. As a result, sufficiently long records should allow separation of such incoherent (free) internal tides (icIT) from deterministic motions. In contrast, recent evidence suggests that considerable open-ocean (far from the source) baroclinic tidal energy (8–26% of barotropic tidal energy according to Dushaw et al. 1995) appears in low-mode motions phase-locked to the barotropic tide (Chiswell and Moore 1999; Ray and Cartwright 2001). More commonly, such coherent internal tides (cIT) are found near their source areas, appearing as ray patterns of enhanced internal tidal energy near sloping topography (Horn and Meincke 1976; DeWitt et al. 1986; Pingree and New 1991; T. Gerkema, personal communication, 2003). At fixed

Responsible Editor: Roger Proctor

H. van Haren
Royal Netherlands Institute for Sea Research (NIOZ),
PO Box 59, 1790 AB Den Burg, The Netherlands
e-mail: hansvh@nioz.nl

positions in such source areas quasi-deterministic narrow-band baroclinic spectra may be observed, making it difficult to separate cIT from BT, that also vary strongly horizontally in such areas. On the other hand, numerical models of motions in shelf-slope regions demonstrate the large effects of complex topography and (small) variations in density on internal tidal variability (Xing and Davies 1997, 1999; Gerkema 2001).

In this paper, we investigate the representation of icIT in the semidiurnal frequency band observed in the deep Bay of Biscay, where icIT amounts to ~30% of BT (and/or cIT). Semidiurnal tidal motions dominate the currents, although near-inertial motions are nearly as energetic (van Haren et al. 2002). The aim is to gain some insight in the nature of observed icIT, in the possible effects of varying background conditions on the varying registration of IT using instruments fixed in space. Since icIT can be considered as spectral background for barotropic tides, the approach in the present study of current meter observations has analogy with historic tide gauge data analyses on tidal cusps (Munk et al. 1965; Munk and Cartwright 1966; Rossiter and Lennon 1968). The non-linear interaction of shallow water tides and the low-frequency continuum was suggested responsible for the enhanced spectral continuum (cusps) surrounding the harmonic constituents (Munk et al. 1965). The simple models presented in this paper also consider several instrumental errors and the spectral representation of sudden jumps in signals passing sensors fixed in space, known as fine-structure contamination (Phillips 1971; Reid 1971).

## 2 Data handling

Spectra were evaluated using 11 months' Aanderaa RCM-8 current meter observations from 1000-m-long subsurface moorings down the continental slope in the Bay of Biscay (Fig. 1). The main focus was on records from two depths (z = -3810 and -4210 m) at the deepest mooring (BB8) at 45°48′N, 06°′50′W ($f = 1.437$ cpd). Local water depth $H = 4810$ m. The foot of the rugged continental slope was about 100 km to the northeast. As background $N \approx 8$ cpd, BB8 was well outside the internal Rossby radius NH/f ~30 km from the shelf edge. In the array BB1–8 down the continental slope, BB8 was furthest from complex topography, in an environment with a near-monochromatic low-frequency (~0.01 cpd) current outside the internal wave frequency band. Note that the real topography is more complex than the smoothed contours in Fig. 1 (cf. Gemmrich and van Haren 2001 for detail). For direct reference, current meter records were also used from $z = -4510$ m on BB8 and from $z = -3715$ and –4115 m at the nearest mooring (BB7; $H = 4715$ m) 50 km towards the continental slope. For further reference, data were used from current meters moored higher up the slope ($H = 2000$ m; BB2) and from a 75-kHz acoustic Doppler current profiler ranging between $-1100 < z < -700$ m (ADCP; BB1; $H = 1600$ m). All current meters stored vector-averaged data every 20 min, the ADCP every 15 min.

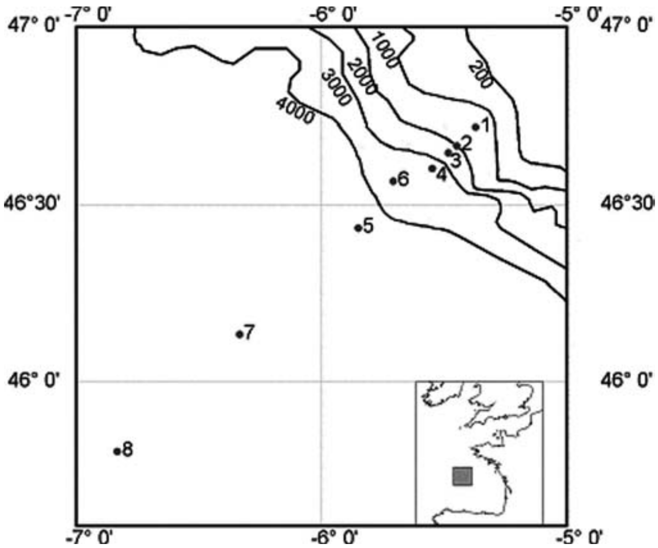


**Fig. 1** Site of moorings 1–8 in the Bay of Biscay (named BB1–8 in the text) with depth contours (m), smoothed across ~10 km horizontally. The relevant scales of the rugged topography are an order of magnitude smaller (Gemmrich and van Haren 2001)

In the spectral analyses performed here the number of degrees of freedom (df) was generally kept very low (df ≈ 3 using a single Kaiser window taper over the entire record) to resolve most of the harmonic frequencies at the expense of a high-accuracy error estimate. Thus, the most energetic internal wave motions were considered as quasi-deterministic, like tides modified by slowly varying background conditions (e.g. Munk et al. 1965), rather than a realization of a (random) stochastic process. As a result, further spectral averaging was not required (Jenkins and Watts 1968).

In order to find icIT we separated the purely deterministic current signal from the observed record by applying a sharp harmonic filter, specifying the frequency of the particular constituent (Dronkers 1964). For year-long records of zonal current component $u$ we defined deterministic currents $u_0$ as the summation of a series of semidiurnal tidal currents at harmonic constituent frequencies:

$$u_0 = \sum_n U_n \cos(\varphi_n + \sigma_n t),$$

$$\sigma_n = 2N_2, \mu_2, N_2, \nu_2, M_2, L_2, S_2, K_2$$
$$(1.83 < \sigma_n < 2.03 \text{ cpd}) \qquad (1)$$

for amplitudes $U_n$ and phases $\varphi_n$, similar for $v$. Frequency ($\sigma$) was given in cycles per day (1 cpd $= 2\pi/86400\ \text{s}^{-1}$). The constituents in Eq. (1) were chosen because they explained more than 99% of the surface pressure gradient-driven semidiurnal equilibrium tidal variance (e.g. Schuremann 1941; Amin 1985; Franco and Harari 1991). Generally, $u_0$ were thought sufficient for separating BT from IT. In Appendix A, however, an example is given of observations proving that Eq. (1) did not always separate BT from cIT. Also, in the case of (the weak constituent) $\mu_2$, an additional contribution can be expected from $2MS_2$, which has the same frequency but is generated by non-linear effects (that will be discussed later) (Kwong et al. 1997). As a result, baroclinic icIT currents were defined as:

$$u_1 = u - u_0 \ , \tag{2}$$

similarly for v. Because BT and cIT were not separable using Eq. (1), the definition Eq. (2) was compared with another common definition of a baroclinic current (e.g. Holloway et al. 2001), being the difference between two records separated vertically by a distance $\Delta z$ ($\Delta$ indicating a finite difference):

$$u_2 = u(z) - u(z + \Delta z) \ , \tag{3}$$

and similarly for $v$. This definition (actually for vertical current shear, when divided by $\Delta z$) yielded $\mathrm{icIT} + \mathrm{cIT}(Z)$. Here, cIT had average scale height $Z \sim< 2\Delta z$, so that $\mathrm{BT} + \mathrm{cIT}(Z \gg \Delta z)$ were associated with $[u(z) + u(z + \Delta z)]/2$. As a result, for $\mathrm{cIT}(Z < 2\Delta z)$ Eq. (3) still contained narrow-band tidal signals and differed greatly from Eq. (2). In that case, ellipse parameter properties (Gonella 1972; Fu 1981) were invoked for discrimination. For example, for free internal waves ($f < \sigma < N$, $N \gg f$, $f$ the local inertial frequency and $N$ the buoyancy frequency) current ellipticity $\varepsilon \sim |f/\sigma|$ (Fu 1981). As a result, $\varepsilon$ has a fixed value for internal waves at a particular frequency (and latitude). In contrast, barotropic (tidal) waves attain eccentricity $\varepsilon = 0$ near a vertical boundary and values varying between $0 < \varepsilon < 1$ in semi-enclosed seas and above sloping, complex topography. Results from barotropic numerical models were not used to define barotropic currents, because their values were not more accurate (5–10% in amplitude; e.g. Kwong et al. 1997) than achieved here.

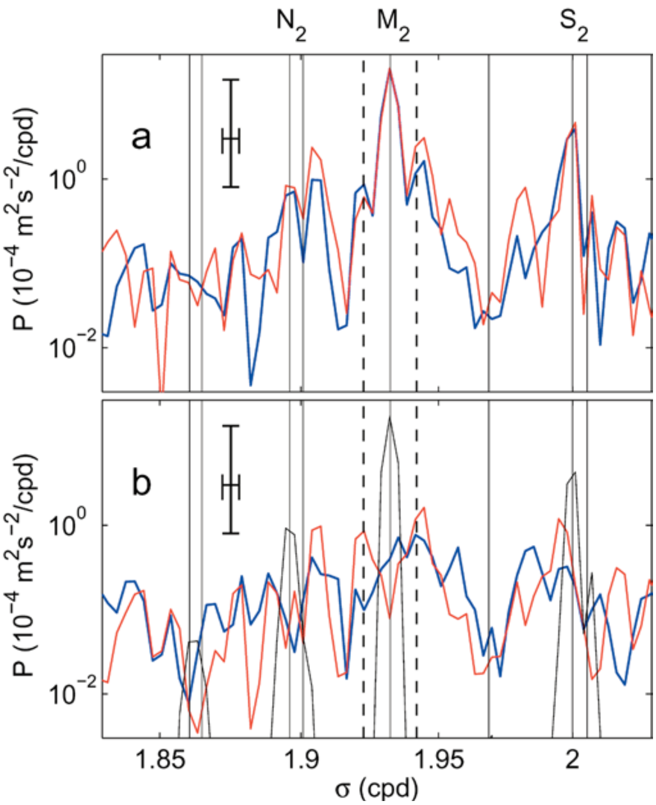


**Fig. 2** **a** Semidiurnal tidal band of nearly unsmoothed ($\nu \approx 3$ df; degrees of freedom) kinetic energy spectra from 11 months of current meter observations at $z = -3810$ m (blue) and $z = -4210$ m (red) a + BB8. At $\nu \approx 3$ df spectra have a frequency resolution of 0.006 cpd, which is indicated with the 95% confidence level inferred from a random statistics model. It is noted that such statistics are not applicable for tidal analysis. Thin vertical solid lines indicate tidal constituents from left to right: $2N_2, \mu_2, N_2, \nu_2, M_2, L_2, S_2, K_2$. Dashed lines indicate $0.995M_2$ and $1.005M_2$. **b** Two ways to separate baroclinic signal from the original records in **a**. The red spectrum is for $\mathbf{u}_1$ $z = -3810$ m according to Eq. (2). The blue spectrum is obtained for $\mathbf{u}_2$ following Eq. (3). For reference, the harmonic barotropic part (Eq. 1) is given in solid black graph

## 3 Observations

Above the abyssal plain, the semidiurnal tidal band typically showed dominating constituents $M_2, S_2$ and $N_2$ as strongly deterministic signals by their spiked, narrow-band appearance (Fig. 2a). In contrast with observations higher up the continental slope (Appendix A), these signals were vertically dependent over the range of observations, because the records from instruments lower by $\Delta z = -400$ (Fig. 2a) and $-700$ m (not shown) yielded essentially the same spectrum. The spectrum of baroclinic motions $\mathbf{u}_2$ showed a different picture: the tidal spikes were gone and a broad, rather flat semidiurnal band remained (Fig. 2b, blue spectrum). Most of these large-scale vertical current differences (shear) were at $f$ (not shown) and *near*-$M_2$. Subtraction of persistent currents $\mathbf{u}_0$ (Fig. 2b, black spectrum) removed semidiurnal tidal peaks from the original record, resulting in a spectrum for baroclinic motions $\mathbf{u}_1$ (Fig. 2b red), which was similar to although slightly more spiked, than the $\mathbf{u}_2$ spectrum. At individual frequencies kinetic energy levels in both baroclinic spectra were about equal to deterministic $N_2$ and ~one decade below deterministic $M_2$ at BB8. When integrated over the semidiurnal tidal band between $1.83 < \sigma < 2.03$ cpd, the IT signals $\mathbf{u}_1$ and $\mathbf{u}_2$ contained $30 \pm 10\%$ of the energy of deterministic $M_2$. The familiar spring–neap tidal cycle was not apparent in these signals (Fig. 3), as was considered typical for icIT (Wunsch 1975). Instead of a 14.5-day cycle, amplitude modulations of $|\mathbf{u}_1|$ and $|\mathbf{u}_2|$ both showed large-scale variations having periods of 50–100 days and faster modulations having periods of 5–7 days. In detail, the two IT signals differed. These differences will also be used to find an explanation for the two dominant modulation periods in both signals.

Over the entire record length, the number of fast modulations of 5–7 days periods was about equal for $|u_1|$ and $|u_2|$. This modulation period reflected the semidiurnal

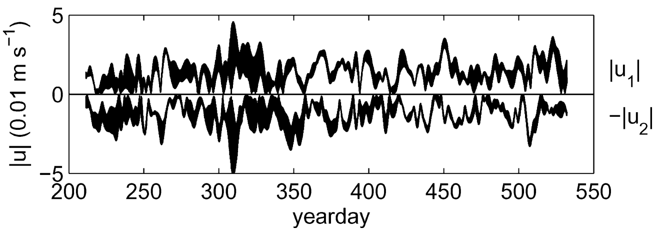


**Fig. 3** Time series of amplitudes of band-pass filtered currents of the two baroclinic semidiurnal tidal signals in Fig. 2b. Filter cutoff frequencies are at 1.79 and 2.11 cpd. *Line thickness* varies due to varying (single harmonic) contributions. Note maximum amplitudes in late autumn. Time is in yeardays according to the convention that 12.00 UTC at January 1 = yearday 0.5, and yearday 365.5 in the second year of observations

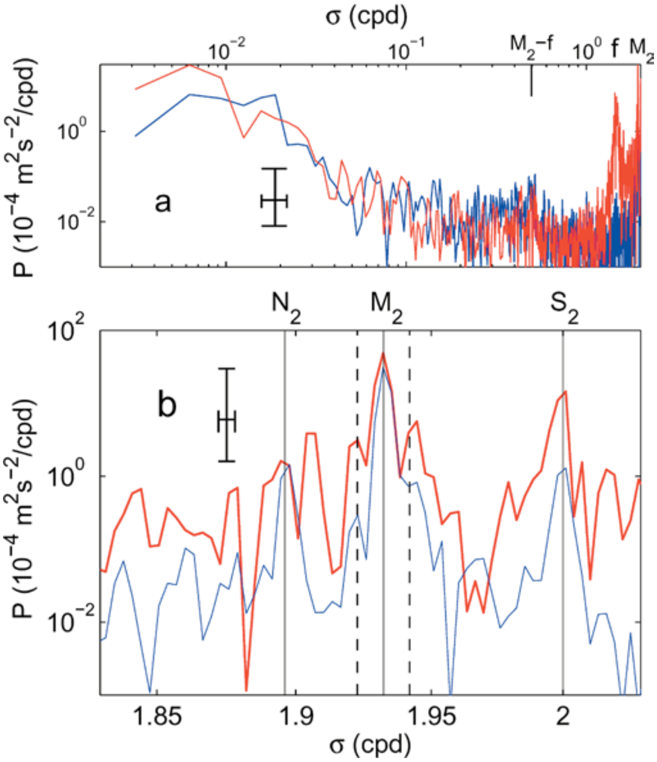


**Fig. 4** **a** Nearly unsmoothed ($\nu \approx 3$ df) rotary spectra for $\sigma \leq 2$ cpd from original current meter record at $z = -3810$ m. The clockwise spectrum (*red*) dominated the anticlockwise spectrum (*blue*) strongly near and above the inertial frequency. **b** Semidiurnal tidal band detail of spectra in **a**. *Thin vertical lines* indicate from left to right: $N_2, M_2, S_2$. *The dashed lines* indicate $0.995M_2, 1.005M_2$

IT band's flatness and width, $\Delta\sigma = 0.09 \pm 0.02M_2$, between frequencies at which the moderately smoothed spectrum was 0.1 of the peak value. Harmonic analysis did not remove energy at non-tidal constituent (sidelobe) frequencies like (0.995, 1.005)$M_2$, nor around $S_2$ or $N_2$. This energy was part of the flat semidiurnal IT band. The $M_2$ sidelobes are used to investigate how and why this band was filled to acquire its relatively large energy and its rather flat shape in frequency. Some of the non-tidal peaks remaining after removal of the deterministic part of the signal were (partially) reduced using Eq. (3) and were thus coherent over at least 400 m vertically. As a result, they did not appear to be a spectral artefact. Note that the energy at these frequencies extended more than three decades above the level of instrumental white noise, similarly to earlier findings in tide gauge records (Munk and Cartwright 1966). Such a small influence of artificial instrumental errors was confirmed using a simple drag–buoyancy force model to investigate the effects of mooring motion. Additionally, a model was studied on mechanical current meter behaviour in weak flows (Appendix B).

Lack of dominance of artificial mooring influence over internal wave motions was confirmed from inspection of rotary spectra (Fig. 4). These spectra showed a generally larger clockwise (−) than anticlockwise (+) circular component, with largest spectral densities ratio $P_-(\sigma)/P_+(\sigma) \gg 1$ near $f$. This ratio slowly decreased at higher internal wave band frequencies as in (Fu 1981), except at some tidal constituent frequencies ($M_2, N_2$). At the latter frequencies, the almost degenerate (rectilinear) current ellipses were evidence of lack of dominant free internal tidal waves emanating from the proposed generation near the shelf break (Fig. 5; Pingree and New 1991; T. Gerkema, personal communication 2003). For free internal waves $P_-(\sigma)/P_+(\sigma) = (\sigma + f)^2/(\sigma - f)^2 \approx 30 - 50$, for the semidiurnal tidal band (Fu 1981). Outside $M_2$ and $N_2$ ratios were observed varying between 10 and 100, also at frequencies like (0.995, 1.005)$M_2$. However, no direct internal wave generation occurred at these non-tidal frequencies. As will be discussed in Section 5, the frequency change from tidal constituents suggested (non-linear) interaction between the internal wave band and variations in background conditions, for example caused by (topographic) planetary waves, having typical periods of O (100) days and, in the short wave limit, having wave lengths of O (100 km) and phase speeds $c \sim O(10^{-2})$ m s$^{-1}$ (LeBlond and Mysak 1978). Motions at such periods dominated the observed sub-inertial (low-frequency) band (Fig. 4a). Below, some qualitative models are discussed which investigate the possibility of such interaction and its spectral presentation.

## 4 Mimicking the spectral presentation of interactions between internal waves and background conditions

In general, a large spectral gap, or rather depression, between $\sim 0.1 < \sigma < 1$ cpd suggested no cascade of energy between planetary and internal gravity waves. However, the relatively large observed baroclinic signals at non-tidal semidiurnal frequencies, causing beat periods of O(50–150 days) of this band in the time domain (Fig. 3), were not accidental, despite our poor spectral statistics. Similar observations were made at different sites above the continental slope (cf. below and in Appendices A and B). In order to explain them, several

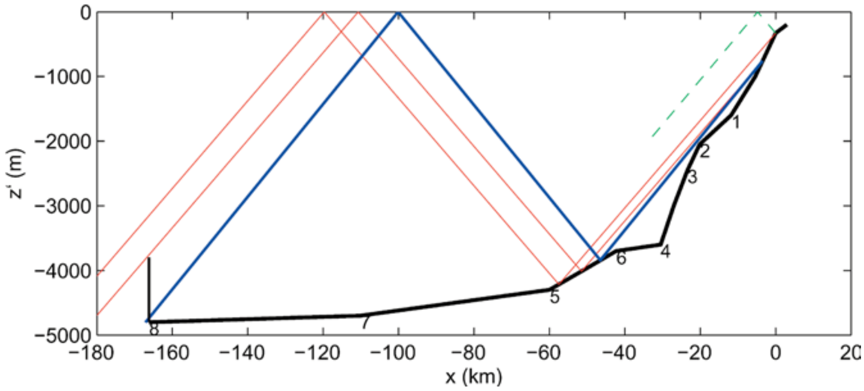


**Fig. 5** Schematic view of effects of topography and background variations on dominant internal wave motions propagating in rays (*colour lines*) passing a fixed mooring (BB8; *vertical black line* indicates the 1000-m vertical extent). The vertical coordinate $z' = z$ for the actual bathymetry in a straight line between BB1–8 (Fig. 1), whilst it indicates a stretched coordinate $z' = z\mathrm{N}(z)/\mathrm{N}_0 + z_0$, with $N_0$ and $z_0$ arbitrary constants, for stratification so that straight lines can be drawn for wave rays. These rays closely represent observed and modeled rays as presented by Pingree and New (1991; henceforth PN), Gerkema (2002) and Gerkema et al. (2003; GLM). Gerkema (2002) found for a combined $M_2 - S_2$ ray pattern a first bottom hit at ~70 km from the source, instead of 50–60 km as in PN and GLM for monochromatic (~$M_2$) waves. Here, the *red beam of rays* represents the width and reflection points of $M_2$ waves. The first reflection at a sloping bottom results in a doubling of the beam width to the seaward side. This beam just reaches the top of mooring 8. A 5% change in N results in a (*blue*) ray that just misses the mooring, but now at its continental side. The near-surface summer stratification results in a second beam of (*dashed green*) rays, complexing further. As a result, the apparent missing of rays of mooring 7 in the present figure is probably not realistic

artificial spectra were considered. These spectra were constructed from time-series models describing signals of time-varying frequency.

Following Kunze (1985), who formulated the effects of a large-scale eddy on internal wave propagation, and inspired by the non-linear instrumental error model in Appendix B, the effects of varying background conditions were studied on propagation of internal waves. As no observations were available for all of the year-long variations of the entire environment, only qualitative results were pursued. Assuming internal (tidal) waves propagated along rays (Fig. 5), their angle $\alpha$ towards the horizontal varied along their path through varying conditions as it depended on effective inertial frequency $f_e(x,y,t)$ and buoyancy frequency $N_e(z,t)$,

$$\sin^2\alpha = (\sigma^2 - {f_e}^2)/({N_e}^2 - {f_e}^2)\ , \qquad (5)$$

where $f_e = f + 1/2\zeta(x,y,t)$ included low-frequency vorticity $\zeta$ of the medium and $N_e = N(z,t) + F(\partial\rho/\partial x, \partial\rho/\partial y) \approx N(z,t)$ (Mooers 1975; Kunze 1985). Relative variation in $f_e$ or $N$ by only 6% had the same effect on the ray angle as varying frequencies from $M_2$ to $S_2$, as is easily verified from Eq. (5). In the case of internal tidal waves being predominantly generated in the same source area near the shelf break, $f_e$ or $N$, relatively varying by ±1%, caused rays to vary their depth over the entire ray height at BB8, assuming a typical vertical extent of ~200 m (Pingree and New 1991, T. Gerkema, personal communication, 2003). As $\alpha$ varied by ~1%, this implied that at a given moment an $M_2$ ray was observed by a current meter, whilst an $S_2$ ray was not, and vice versa at other moments. If $f_e$ or $N$ relatively varied by ±2.5% as for the blue ray in Fig. 5, the rays varied by more than the entire 1000 m mooring length at BB8.

*Locally*, we observed such variations in background conditions even from our poorly resolved mooring arrays (Fig. 6). Low-frequency ($l; \sigma < 0.05$ cpd) stratification varied by $(\Delta N/N)_l \approx \pm 3\%$ over 400 m vertical distance (Fig. 6a). The amplitudes of low-frequency current components varied by ~0.04 m s$^{-1}$ between BB7-BB8, so that $\Delta(u,v)_l/\Delta(x,y) \sim \pm 0.01f$ per component (Fig. 6b). As a result, the above sketched relative variations in $f_e$ or $N$ were potentially sufficient to cause low-frequency variations in internal tidal rays over the entire mooring length at BB8, provided the relative variations in the area between source and mooring were similar to the observed local values.

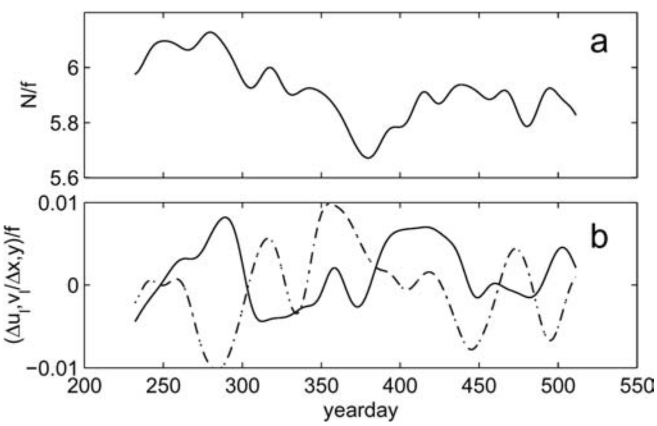


**Fig. 6** **a** Low-pass filtered (cutoff at ~ 0.05 cpd) time series of $N = (\alpha g/\rho\Delta T/\Delta z)^{0.5}$ from temperature records from current meters at $z = -3810$ m and −4210 m (BB8), using $\alpha = 0.16$ thermal expansion coefficient (inferred from the T–S relationship in CTD observations). **b** Low-pass filtered time series of differences between current components $\Delta u$ (*solid*), $\Delta v$ (*dashed*) at $z = -3810$ m (BB8) $z = -3710$ m (BB7) across horizontal distances $\Delta x, \Delta y \approx 37$ km. Values of N and horizontal shear ($\Delta u/\Delta x$ etc) are normalized by local $f$

Unfortunately, a quantitative relationship explaining internal tidal intermittency could not be given as variations in background conditions were not known for the entire area. Similarly, it was not possible to relate the locally observed changes in background conditions to specific forcing, like atmospheric forcing, as suggested using a numerical model by Xing and Davies (1997). However, a suggestion for the spectral presentation of intermittency can be given.

Considering a plane wave motion,

$$u(x, y, z, t) = Ue^{i(kx+ly+mz-\sigma t)} \ ,$$

in a frame of reference of an internal wave ray, satisfying the dispersion relation in Eq. (5) and which was considered at a fixed spot in space as:

$$u(t) = U(t)e^{-i[\sigma t+\varphi(t)]} \ , \tag{6}$$

with phase $\varphi(t)$, the effects of time-dependent $f_e$ and $N$ were modelled in two different ways to describe the spectral appearance of varying tidal current amplitude and phase. The two (arbitrary) models described changes in $U$ and $\varphi$ as if governed by (sudden) changes in internal wave ray position due to subinertial variations in background conditions.

In the first model, sudden changes in ray position with respect to an instrument fixed in space occurring only a few times a year (~0.01 cpd) could create sudden current changes as in the example observed passing our fixed mooring (Fig. 7a). The first half of this 1-week record was dominated by a few harmonic frequencies, whilst the second half by many harmonics so that amplitude and phase varied more abruptly. The main transition was like a step function at day 301.5, during reversal of the low-frequency current. To model this, we considered simple artificial records mimicking a scalar velocity component at a single frequency ($\sigma = M_2$),

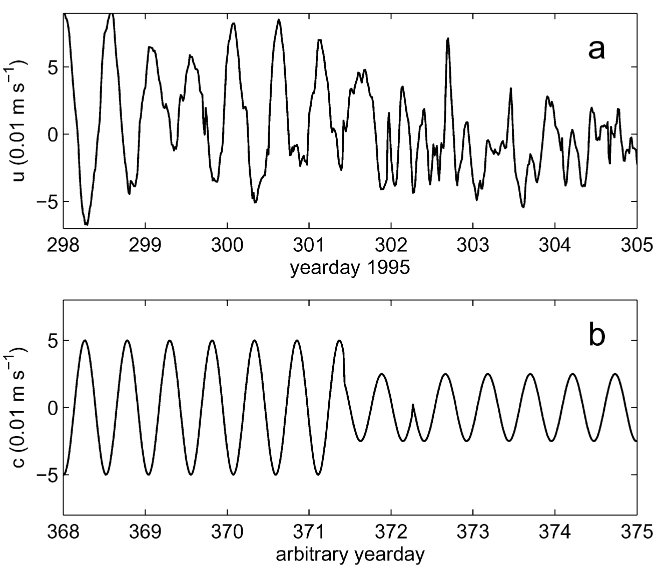


**Fig. 7 a** One-week example of time series of unfiltered $u$-current component observed at $z = -3810$ m. **b** Detail of artificial time series (Eq. 7b) showing the sudden current transition

$$a(t) = \cos \sigma t, \text{ for } 0.375T < t < 0.51T,$$
$$a(t) = 0 \text{ otherwise}, \tag{7a}$$
$$c(t) = a(t) - b(t)/2, \text{ with } b(t) = \cos \sigma t$$
$$\text{for } 0.5T < t < 0.625T, \ c(t) = 0 \text{ otherwise}, \tag{7b}$$

where $T = 333$ days denoted the record length, which was taken equal to the length of our observations. The artificial time series were non-zero well away from the end points of the records to avoid smoothing effects by the pre-FFT taper window. The two series (8a,b) had two non-zero jumps in common at the transition from the zero-padding to non-zero signal. The difference between the two was a single amplitude and phase jump between two identical harmonics in the middle of the composite record $c(t)$ (Fig. 7b). This $c(t)$ was constructed to mimic the switch between, superposition of, two motions of identical frequency but opposite phase, as if an internal wave ray had entirely moved passed the instrument. Models by Pingree and New (1991) and T. Gerkema, (personal communication, 2003) show 90–180° phase difference across the width of a ray.

The spectrum of $a(t)$ showed a broad peak at its central frequency having a width as expected from its non-zero record length of $\sim 1/8T$ (Fig. 8a). The non-zero sidelobes were entirely attributable to the two transitions at the beginning and end of non-zero signal, reflecting a rectangular taper window (Jenkins and Watts 1968). The more interesting record $c(t)$ lost its peak at the central frequency, and redistributed energy into two neighboring peaks at frequencies about the fundamental frequency associated with its non-zero length ($0.25T \approx 80$ days) away from the central frequency. Interpreting observations as in Fig. 2 and others, e.g. from BB7 (Fig. 8c), in terms of model (Eq. 7), some four to five major jumps as in Fig. 7b were expected in a 11-month record. This number was close to the observed number of sign changes in the dominating low-frequency currents. Model Eq. (7) mimicked enhancement of neighbouring frequencies up to $\pm 0.02$ cpd around $N_2, M_2, S_2$. However, it did not explain apparent asymmetrical shape of such frequency bands around $N_2, S_2$.

The second model considered a time-varying ray as a slow sinusoidal variation with time of the phase in Eq. (6), so that the simple scalar velocity component $d(t)$ modelling $u(t)$ at a single frequency read:

$$d(t) = D\cos(\sigma t + d_l \cos \sigma_l t), \quad \sigma_l \ll \sigma \tag{8}$$

for adjustable phase-amplitude $d_l$ and frequency $\sigma_l$. The Fourier transform of this model resembled Bessel functions of the first kind (Arfken 1970), in which the ratio $\sigma/\sigma_l = v$ the order of Bessel function, and $d_l$ determined the spectral width in frequency.

We examined Eq. (8) for $\sigma = M_2$ using only a single low-frequency $\sigma_l = 0.01$ cpd (Fig. 8b). For small amplitude $d_l = 0.2$ Eq. (8) resembled model $c(t)$ in Eq. (7), with the exception of a peak remaining at the central frequency (blue spectrum in Fig. 8b). For larger

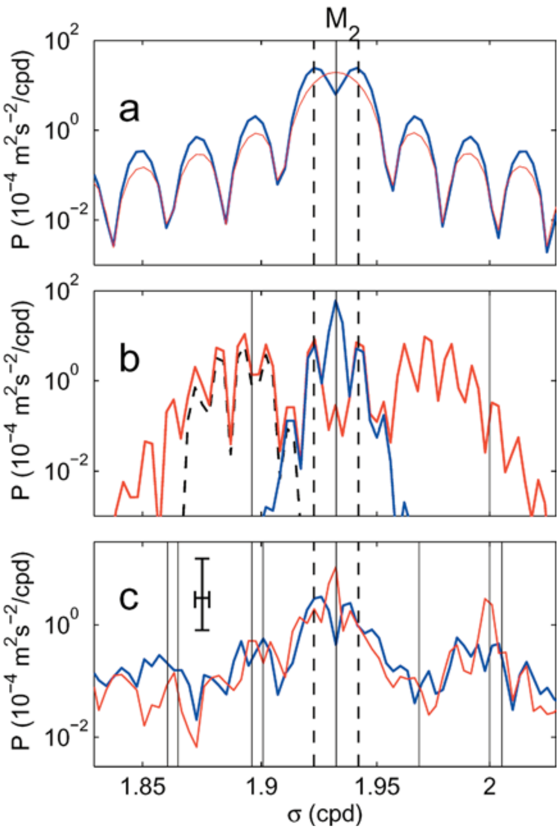


**Fig. 8** **a** Spectra of artificial velocity record (Eq. 7a) in *red* and (Eq. 7b) in *blue*. **b** Spectra of artificial velocity record $d(t)$ in Eq. (8) using $d_l = 0.2$ (*blue*) and 1.7 (*red*). The slightly offset spectrum in *dashed black* indicates the sharp elliptic filter cutoff frequencies around $N_2$. **c** *Red spectrum* as Fig. 2a, but for $z = -3714$ m at mooring BB7 (*red*). The *blue spectrum* represents $\mathbf{u}_2$ (Eq. 3) as in Fig. 2b, but for BB7

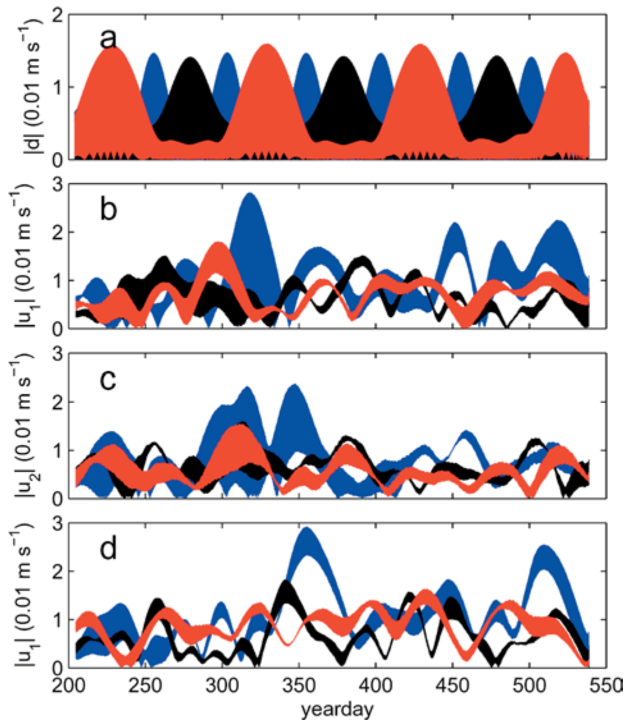


**Fig. 9** **a** Time series of band-pass filtered artificial series (Eq. 8) using $d_l = 1.7$. The elliptic filter cutoff frequencies are $\pm 0.02$ cpd around $N_2$ (*red*), $M_2$ (*blue*), $S_2$ (*black*). **b** As **a** but for baroclinic series (Eq. 2) from observations at $z = -3810$ m at BB8. **c** As **b** but for baroclinic series (Eq. 3). **d** As **b**. but for observations at $z = -4510$ m

amplitudes, the spectrum widened as expected, filling the entire semidiurnal frequency band for $d_l = 1.7$ (or $\sim$1/4 period; i.e. $\sim$the ray width in Pingree and New 1991; $\sim$the core of the ray in T. Gerkema, personal communication, 2003) (red spectrum in Fig. 8b). In the latter case, a gap was found at the central frequency and the spectrum was mirror-symmetric around it. Assuming low-frequency vorticity generating the sinusoidal phase changes ($d_l = \Delta(u, v)_l$), the above amplitudes implied horizontal scales (wavelengths) of low-frequency motions of 300 and 40 km, respectively. These values were comparable to those of baroclinic planetary waves. Further distinction, for example between the two models of different $d_l$, was not possible, because we did not have independent estimates of the spatial scales of low-frequency variability. The comparable results of the simple models Eqs. (7) and (8) implied that a realistic phase slowly (non-linearly) varying with time, could have induced the observed broadening (and flattening) of the observed icIT spectral signal.

Model (Eq. 8)'s property to fill the semidiurnal band caused beat periods of the motions within separable bands around the three main lobes (around $N_2, M_2, S_2$) to be mutually exclusive in the time domain. This was visible in Fig. 9a, after filtering data using sharp elliptic filters twice, back and forth (as shown for $N_2$ by the black dashed spectrum in Fig. 8b). This mutual exclusive property of the main semidiurnal tidal bands was also seen in the observations (Fig. 9b, d), although differently for different data. Physically, this same result could be obtained if narrow IT beams of different frequency were separated in space and thus passed a mooring independently. This was suggested after comparing the observations in Fig. 9b and d, for instruments on the same mooring separated by 700 m vertically. The modulation of all three components varied differently with time. Adopting this as typical for icIT intermittent signals, their spectral signature revealed a gap at their central frequency. Bearing that in mind and comparing Fig. 9b and c, it is seen that method (2) separated different icIT frequency bands better from observed currents than method (3). Apparently, (some) shear across relatively short spatial scales incorporated in Fig. 9c smeared mutual frequency bands, so that the result was a more flat spectrum, as noted previously in discussing Fig. 2.

## 5 Discussion and conclusions

Semidiurnal tidal band observations were studied in an attempt to separate large-scale tidal motions from motions that varied over relatively short scales. It was shown that the semidiurnal tidal currents in the deep Bay of Biscay were dominated by very narrow-band signals at three frequencies ($M_2, S_2$ and $N_2$). The ellipticity of these motions was almost rectilinear at $M_2$ and $N_2$, whilst nearly circular for $S_2$. Although the ellipticity observed at $S_2$ approached free internal wave ellipticity (Fu 1981), the others did not. This suggested strong spatial variability as in interference patterns of different waves, like Poincaré modes for barotropic tidal waves in a semi-enclosed basin such as the North Sea (LeBlond and Mysak 1978). Although not all relevant spatial scales were resolved, it was concluded that these narrow-band observations represented large-scale ($\Delta z > 1000$ m) baroclinic motions on which variations in background stratification had little effect, or, more likely, they represented depth-independent topographically modified barotropic motions. The latter confirmed previous studies by Hendry (1977).

In contrast, small-scale variability was associated with a broad band of frequencies covering the entire semidiurnal tidal band. Such baroclinic icIT motions comprised ~30% of the energy supported by the large-scale tidal constituent motions. This value was slightly larger than reported by Dushaw et al. (1995). The icIT motions were not removed using harmonic analysis because most were observed at non-tidal constituent frequencies in a Eulerian frame of reference. Models suggested that icIT were due to (non-linear) interaction between internal wave motions and varying background conditions, such as caused by planetary waves. These varying conditions caused occasional sudden current variations passing the moorings. This seemed similar to fine-structure contamination, which led to more general analysis of typical internal wave band spectral falloff rate of $P(\sigma) \sim \sigma^{-2}$ (Phillips 1971; Reid 1971). However, in the present study on the semidiurnal band it was shown that icIT was flat rather than sloping with frequency and it had ellipse properties of internal waves, indicative of non-random (spectral) signals. Due to their dependence on non-randomly varying tidal and background conditions, this suggests that icIT are better described by treating these signals as (quasi-) deterministic rather than purely stochastic.

Some of the presented observations (Appendix A) also showed that near their source at the shelf break internal tidal signals were persistent over an entire year. There, internal tidal spring–neap cycles were observed. These cycles lead to spring–neap cycles in soliton formation near the thermocline (Gerkema 2001), which may lead to low-frequency variations in mixing and associated varying N, and thus different ray paths. Since the mooring analyzed here is O(100 km) away from the assumed source of IT, the likelihood that the spring–neap cycle of forcing at the generation site will be observed consistently throughout the ~1 year of data is small. As was discussed, large-scale variations in $f_e$ and $N$, by the amount as observed locally, cause the relative positions of the $M_2$- and $S_2$-internal tidal ray paths to vary relative to each other, and to the mooring location. Such variation already appeared between different models (Pingree and New 1991; T. Gerkema, personal communication, 2003), most likely due to small changes in topography or N, as demonstrated by Gerkema (2002). Not considered in these models or in the present study are the effects of small (canyon-scale) topography (Munk 1997) and the effects of variations at small subtidal scales, for example introduced by near-inertial motions. The latter generate large shear and thereby possibly large variations in $N$. This suggests a complex interaction relationship between (near-inertial) background variations and internal tidal motions and a filling of the internal wave spectrum in bands (van Haren et al. 2002; van Haren 2003)

The expected result of the interaction between tidal and low-frequency variability is a smearing of the initially discrete spectra in the semidiurnal band, across the entire semidiurnal band and perhaps beyond. The low-frequency variations caused the relatively flat spectral response and internal tidal intermittency, which varied over short scales although not (necessarily) being due to a random stochastic process. As a result, spectral averaging of different records (in space or time) implied inappropriate averaging of non-random physical signals. Although the focus was on the semidiurnal band, it was noted that these tidal interaction signals were generating not only icIT, but also the rest of the continuum spectrum, usually referred to as the red noise ocean spectrum. This noise extended ~three decades above background instrumental (white) noise. The present current meter observations study confirmed (the tide gauge study by) Munk et al. (1965), who contemplated that "one could study low-frequency [climate] fluctuations [from this noise spectrum] even if the recording instruments do not have the prerequisite long-term stability". This requires further study of longer (current meter) records, although some seasonal variability is apparent in Fig. 3.

**Acknowledgements** I enjoyed the assistance of the crew of the *R/V Pelagia* in the deployment and recovery of all moorings. I thank Leo Maas for ongoing discussions. Margriet Hiehle designed Fig. 1. I thank Hendrik van Aken for the use of current meter data from his TripleB project in the Bay of Biscay, which was supported by a grant from The Netherlands Organization for the Advancement of Scientific Research, NWO.

## Appendix A. Observations of coherent baroclinic tidal motions

Year-long current meter records can be insufficient to distinguish between barotropic and persistent or coherent baroclinic motions, as we show in the example below. Up the continental slope, in $H = 1600$ m water depth, an upward-looking 75 kHz narrow-band ADCP was moored at $z = -1100$ m. It had a nominal range of 400 m (~25% of the water column) and sampled 25 bins of 16 m. Despite the observations spanning an entire cycle of seasonal thermocline near the surface, the amplitudes and phases of the dominant $M_2$ current components varied strongly over 200–300 m vertically near mid-depth (Fig. 10). This vertical current structure clearly indicated baroclinic motions, despite their persistence with time as inferred from the sharp spectral peak (Fig. 10b). Baroclinicity was also suggested from the eccentricity of the current ellipse (Fig. 10a), approaching linear internal wave values.

Apparently, these observations were from a site near the source of internal tidal wave generation, assumed to be the shelf break by Pingree and New (1991). Otherwise, it was hard to explain that year-long variations in density, especially those within the seasonal thermocline, had no effect on the deterministic presentation of baroclinic cIT (Gerkema 2001). It was clear that at such locations much longer records were needed to separate (topographically modified) BT from cIT, as the proper vertical scales (the entire water column) were not resolved.

It was inconclusive whether the deterministic observations above the abyssal plain (Fig. 2) were attributable to BT or cIT. To be sure, one needed longer records. However, the current ellipses observed there were nearly rectilinear (cf. Fig. 10a), with major axis directed along the main isobaths. This confirmed earlier observations by Hendry (1977), who found predominantly BT at a similar location. Also, these observations were so far from the main internal tide source near the shelf break that slow variations in stratification, as in the seasonal thermocline, were expected to strongly influence internal wave propagation, according to modelling results by Gerkema (2001, 2002).

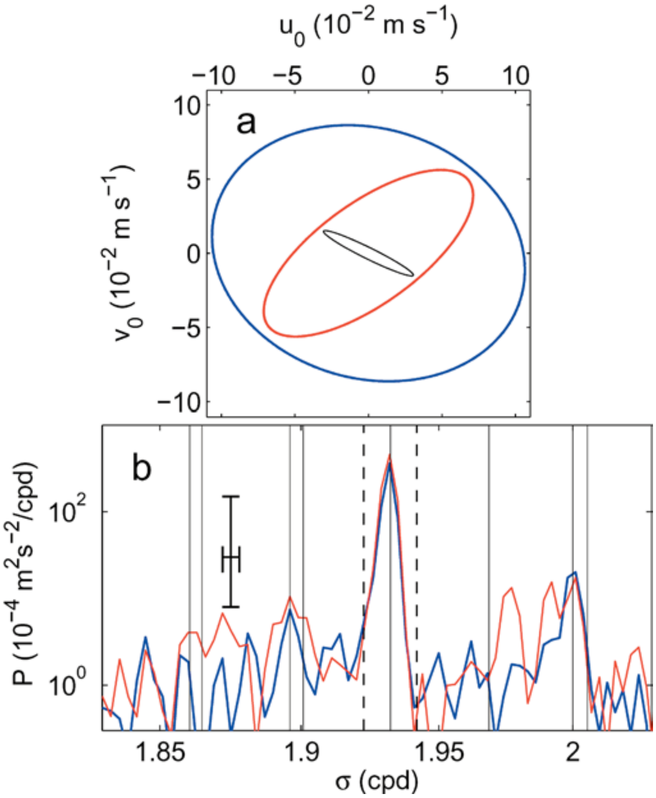


**Fig. 10** **a** Harmonic $M_2$ ellipses measured by 75 kHz ADCP (BB1; $H = 1600$ m) at $z = -725$ m (*red*) and $z = -980$ m (*blue*). For reference the ellipse measured at $z = -3810$ m at BB8 is given (*black*). Current ellipses are adjusted for magnetic deviation (~ 6°W), and the local mean direction of the isobaths is approximately in the direction of the major axis observed at BB8. **b** The *blue spectrum* is for ADCP (BB1) data measured at $z = -980$ m, the *red spectrum* for the difference between currents measured at $z = -820$ and −980 m. The *thin vertical lines* are as in Fig. 2

## Appendix B. Spectra from mechanical current meters in weak flows

In the lower 1000 m above the bottom of the abyssal plain (BB7,8) maximum current speeds never exceeded 0.12 ms$^{-1}$ and 10% of the data fell below the threshold value of 0.02 ms$^{-1}$ for Aanderaa's RCM-8 mechanical current meters (Fig. 11a). The (spectral) influence of these erroneous 10% of the data was tested on artificial appearance of higher (tidal) harmonics and semidiurnal non-tidal sidebands like $(1.000 \pm 0.005)M_2$. The BB8 observations were compared with RCM-8 and ADCP data higher up the slope in stronger currents, and with artificial data. The artificial data consisted of motions at five harmonic frequencies ($\sigma_1 = 0.007$ cpd, $\sigma_2 = 0.020$ cpd, $\sigma_3 = f, \sigma_4 = M_2, \sigma_5 = S_2$) typical for observed spectra (Figs. 2, 4). To approximate observed characteristics (amplitude, ellipticity), harmonic analysis was performed to compute $(U_n, \varphi_n)(\sigma_n)$, $n = 1, .., 5$ for $u$-component, and $(V_n, \psi_n)(\sigma_n)$ for $v$. The $U_n, V_n$ were enhanced so that the variance at the single harmonic frequencies approximated the variance of the frequency band they represented. Three cases were considered. In all cases Eq. (9a–c) the current speeds were fixed to 0.015 ms$^{-1}$ when they fell below a threshold value (~15% of maximum current in the record, so that 10% of the data was lower than the threshold value),

$$u_a = 1.3 \sum_{j=4,5} U_j \cos(\sigma_j t + \varphi_j), \quad v_a = 0, \tag{9a}$$

$$u_b = 2 \sum_{i=1,2} U_i \cos(\sigma_i t + \varphi_i) + 5U_3 \cos(\sigma_3 t + \varphi_3) + 1.3 \sum_{j=4,5} U_j \cos(\sigma_j t + \varphi_j),$$

$$v_b = 2 \sum_{i=1,2} V_i \cos(\sigma_i t + \psi_i) + 5V_3 \cos(\sigma_3 t + \psi_3) + 1.3 \sum_{j=4,5} V_j \cos(\sigma_j t + \psi_j), \tag{9b}$$

$$|u_c| = |u_b|, D_c = \arctan(u_b/v_b);$$

$$D_c = \pi/2 \text{ when } |u_c| = 0.015 \text{ ms}^{-1} \text{ (truncated)} . \tag{9c}$$

Just truncating the current speed of the realistic case (Eq. 9b) (Fig. 11b) resulted only in a very weak rise of the white noise level to $P \sim 10^{-7}$m$^2$s$^{-2}$/cpd, observed at very high frequencies. In this case, retaining a perfect

Fig. 11 **a** Observed current speed using Aanderaa RCM-8 current meter at $z = -3810$ m (BB8). **b** Artificial current speed for cases (9b,c). **c** Nearly unsmoothed ($\nu \approx 3$ df) kinetic energy spectra for observed current at $z = -3810$ m (BB8; *blue*) and artificial case (9c) (*red*). The *vertical lines on top* indicate $\sigma_1, \ldots, \sigma_5$ in Eq. (9), with $D_2$ indicating $M_2$ and $S_2$. **d** Detail of nearly raw ($\nu \approx 3$ df) kinetic energy spectra for observed current at $z = -1500$ m (BB2; *blue*; offset vertically by factor 0.33) and artificial case (9c) (*red*; offset vertically by factor 3). The *thin vertical lines* are as in Fig. 2

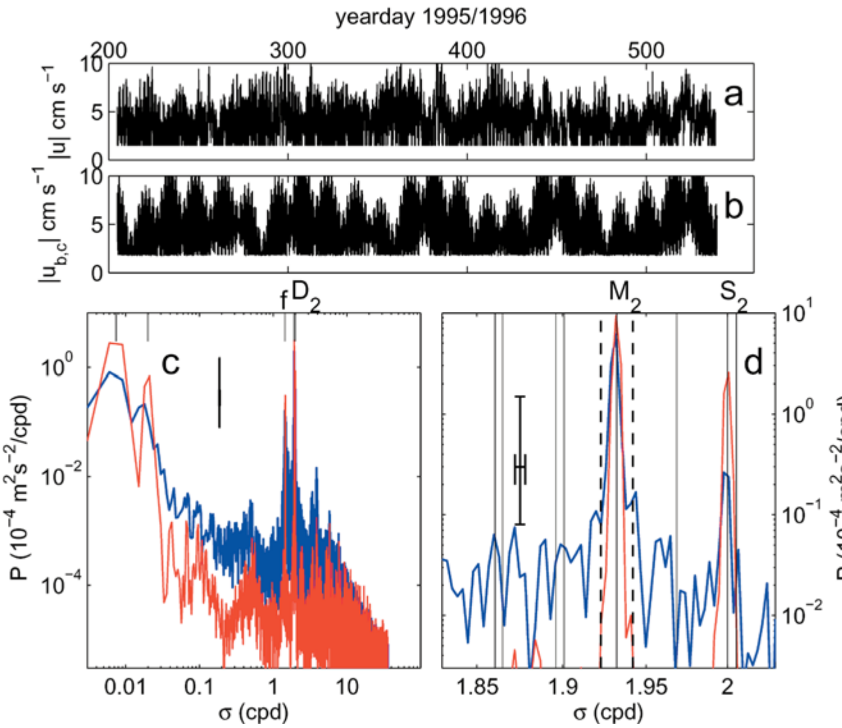


direction measurement, no generation of higher harmonics was observed. In contrast, truncating the speed of purely rectilinear motions (Eq. 9a) resulted in generation of higher tidal harmonics at energy levels approximately of observed $M_6$, more or less constant for the first four higher harmonics (up to $M_{10}$). This case was unrealistic in comparison with observed spectra for $\sigma > M_6$. However, it demonstrated different effects of speed truncation in rectilinear currents, in comparison with currents of mixed ellipticity as in the present observations.

In these observations, instrumental errors did cause (weak) increase of non-linear higher harmonics and noise levels due to delayed response of the current meters' vane upon current reversal in weak flows. This was studied in case Eq. (9c) using an (exaggerated) approximation for such delayed response by fixing direction to an arbitrary value when speed was below threshold value. This case enhanced noise levels by half a decade, so that high-frequency noise was as in the observations (Fig. 11c). It also showed more energy at tidal–tidal and tidal–inertial interaction frequencies, although about one decade lower than observed for $\sigma < M_4$ and reaching observed levels near $\sigma = N \sim 8$ cpd. As a result, the spectral slope of the artificial higher harmonics was quite different from the one observed (van Haren et al. 2002). The model also showed a surprising effect of low-frequency motions: when energy at $\sigma_1, \sigma_2$ was removed in Eq. (9c), noise levels dropped by half a decade and only odd harmonics were enhanced. Like the other cases, case Eq. (9c) also could not explain enhanced motions at frequencies like (0.995, 1.005)$M_2$, which were two decades lower than observed (Fig. 11d; note spectra offset by one decade). It was concluded that (non-linear truncation) errors induced by mechanical current meters could not have caused the observed energy at interaction frequencies between inertial, tidal and subinertial motions. This was confirmed by inspecting observations in stronger flows.

At 500 m above the bottom ($H = 2000$ m; BB2) an Aanderaa RCM-8 current meter returned only 66 (0.27%) of 24,100 current speeds below the threshold level. The kinetic energy spectrum (Fig. 11d) differed from the spectrum at BB8, but this was not attributable to the larger amount of errors in the latter data. Besides similar higher tidal and tidal–inertial harmonics, enhanced values were also observed near frequencies (0.995, 1.005)$M_2$ at BB2. ADCP data ($H = 1600$ m; BB1; Fig. 10) also showed enhanced energy at tidal–tidal and tidal–inertial interaction frequencies. By definition, ADCP data did not suffer from artificial non-linear motions introduced in weak flows. They were only averaged over larger spatial areas.

## References


Arfken G (1970) Mathematical methods for physicists. Academic Press, New York

Amin M (1985) Temporal variations of tides on the west coast of Great Britain. Geophys J Roy Astron Soc 82: 279–299

Chiswell SM, Moore MI (1999) Internal tides near the Kermadec Ridge. J Phys Oceanogr 29: 1019–1035

DeWitt LM, Levine MD, Paulson CA, Burt WV (1986) Semidiurnal internal tide in JASIN: observations and simulation. J Geophys Res 91: 2581–2592

Dronkers JJ (1964) Tidal computations in rivers and coastal waters. North Holland, Amsterdam

Dushaw BD, Cornuelle BD, Worcester PF, Howe BM, Luther DS (1995) Barotropic and baroclinic tides in the central North

Pacific Ocean determined from long-range reciprocal acoustic transmissions. J Phys Oceanogr 25: 631–647

Ekman VW (1931) On internal waves. Rapp Proces Verb Reun Cons Perm Int Explor Mer 76: 5–34

Franco AS, Harari J (1991) Comments on the results of a tidal analysis with a nodal cycle resolution level. In: Parker BB (ed) Tidal hydrodynamics Wiley, New York, pp 737–751

Fu L-L (1981) Observations and models of inertial waves in the deep ocean. Rev Geophys Space Phys 19: 141–170

Gemmrich JR, Haren H van (2001) Thermal fronts generated by internal waves propagating obliquely along the continental slope. J Phys Oceanogr 31: 649–655

Gerkema T (2001) Internal and interfacial tides: beam scattering and local generation of solitary waves. J Mar Res 59: 227–255

Gerkema T (2002) Application of an internal tide generation model to baroclinic spring-neap cycles. J Geophys Res 107: 3124, doi: 10.1029/2001JC001177

Gerkema T, Lam F-PA, Maas LRM (2003) Internal tides in the Bay of Biscay: conversion rates and seasonal effects. Deep-Sea Res II: submitted

Gonella J (1972) A rotary-component method for analysing meteorological and oceanographic vector time series. Deep-Sea Res 19: 833–846

Haren H van (2003) On the polarization of oscillatory currents in the Bay of Biscay. J Geophys Res 108: 3290, doi:10.1029/2002JC001736

Haren H van, Maas L, van Aken H (2002) On the nature of internal wave spectra near a continental slope. Geophys Res Lett 29(12): 10.1029/2001GL014341

Haren JJM van, Maas LRM (1987) Temperature and current fluctuations due to tidal advection of a front. Neth J Sea Res 21: 79–94

Hendry RM (1977) Observations of the semidiurnal internal tide in the western North Atlantic Ocean. Phil Trans Roy Soc Lond 286: 1–24

Horn W, Meincke J (1976) Note on the tidal current field in the continental slope area off Northwest Africa. Mem Soc Roy Sci Liège 6(X): 31–42

Holloway PE, Chatwin PG, Craig P (2001) Internal tide observations from the Australian north west shelf in summer 1995. J Phys Oceanogr 31: 1182–1199

Jenkins GM, Watts DG (1968) Spectral analysis and its applications. Holden-Day

Kunze E (1985) Near-inertial wave propagation in geostrophic shear. J Phys Oceanogr 15: 544–565

Kwong SCM, Davies AM, Flather RA (1997) A three-dimensional model of the principal tides on the European Shelf. Progr Oceanogr 39: 205–262

LeBlond PH, Mysak LA (1978) Waves in the ocean. Elsevier, New York

Maas LRM, van Haren JJM (1987) Observations on the vertical structure of tidal and inertial currents in the central North Sea. J Mar Res 45: 293–318

Mooers CNK (1975) Several effects of a baroclinic current on the cross-stream propagation of inertial-internal waves. Geophys Fluid Dyn 6: 245–275

Munk W (1997) Once again: once again – tidal friction. Prog Oceanogr 40: 7–35

Munk WH, Cartwright DE (1966) Tidal spectroscopy and prediction. Phil Trans Roy Soc (A)259: 533–581

Munk WH, Zettler B, Groves GW (1965) Tidal cusps. Geophys J Roy Astr Soc 10: 211–219

Phillips OM (1971) On spectra measured in an undulating layered medium. J Phys Oceanogr 1: 1–6

Pingree RD, New AL (1991) Abyssal penetration and bottom reflection of internal tidal energy in the Bay of Biscay. J Phys Oceanogr 21: 28–39

Ray RD, Cartwright DE (2001) Estimates of internal tide energy fluxes from Topex/Poseidon altimetry: central North Pacific. Geophys Res Lett 28: 1259–1262

Reid RO (1971) A special case of Phillips' general theory of sampling statistics for a layered medium. J Phys Oceanogr 1: 61–62

Rossiter JR, Lennon GW (1968) An intensive analysis of shallow water tides. Geophys J Roy Astr Soc 16: 275–293

Schuremann C (1941) Manual of harmonic analysis and prediction of tides. US Government Printing Office, Washington, DC

Wunsch C (1975) Internal tides in the ocean. Rev Geophys Space Phys 13: 167–182

Xing J, Davies AM (1997) The influence of wind effects upon internal tides in shelf edge regions. J Phys Oceanogr 27: 2100–2125

Xing J, Davies AM (1999) The influence of topographic features and density variations upon the internal tides in shelf edge regions. Num Meth Fluids 31: 535–577